ELSEVIER

PII: S0032-3861(97)10069-6

Polymer Vol. 39 No. 25, pp. 6577–6588, 1998

0032-3861/98/$ - see front matter

Processing of (in)tractable polymers using reactive solvents. 4: Structure development in the model system poly(ethylene)/styrene

J.G.P. Goossens, S. Rastogi, H.E.H. Meijer* and P.J. Lemstra
Eindhoven Polymer Laboratories/Centre for Polymers and Composites, Eindhoven University of Technology, Den Dolech 2, P.O. Box 513, 5600 MB Eindhoven, The Netherlands
(Received 7 October 1996; accepted 21 August 1997)

The use of reactive solvents provides a unique opportunity to extend the processing characteristics of both intractable and standard (tractable) polymers beyond existing limits. The polymer to be processed is dissolved in the reactive solvent (monomer) and the solution is transferred into a mould. Upon polymerisation, phase separation and phase inversion occur and the originally dissolved polymer becomes the continuous (matrix) phase, whereas the reactive solvent is dispersed as a particulate (thermoset or thermoplastic) phase, hence there is no need for solvent removal. In the present study, the structure development of the model system polyethylene/styrene will be discussed. In situ X-ray studies, SAXS and WAXS, combined with Raman spectroscopy to follow the conversion from monomer to polymer, revealed the importance of liquid–liquid (L–L) *versus* liquid–solid (L–S) phase transformations upon the structure development.

(Keywords: poly(ethylene); styrene; reactive solvent)

INTRODUCTION

The use of solvents is common practice in polymer processing. Solvents are mainly used to avoid high processing temperatures in, for instance, solution spinning of *intractable* polymers like poly(vinylalcohol) (PVAL)[1] and poly(acrylonitrile) (PAN)[2], or to reduce the viscosity during processing of, for instance, ultra-high-molecular weight polyethylene (UHMW-PE)[3,4]. In these processing techniques, however, the solvent has to be removed after processing. This is unfavourable, since the energy required is substantial and in most cases the solvent may even be hazardous, which is increasingly cumbersome in view of environmental legislation. One other drawback of using solvents is the limitation to products with a high surface-to-volume ratio such as coatings, fibres, films and prepregs for composite applications.

A possible solution to overcome some of these problems can be the use of 'solid' solvents, as proposed by Chung and co-workers[5,6]. The concept of 'solid' solvents is to use low-molecular weight crystalline materials (LMC) as a processing aid. In the ideal case, the solid acts as a solvent during processing at elevated temperatures and crystallises from the polymer upon cooling, becoming a non-solvent, which should not affect the final properties of the product. In actual practice, however, the problem usually encountered is the solubility of the residual solvent in the polymer, lowering the T_g and, consequently, inherently affecting those properties[5].

In our laboratory, a novel processing route for (in first instance) intractable polymers was initiated by the use of *reactive* solvents. The intractable polymer to be processed is dissolved at elevated temperatures in a reactive solvent (monomer). The homogeneous solution, possessing a lower viscosity with respect to the pure polymer, is subsequently transferred into a mould and/or fabric. Upon polymerisation in the mould, phase separation and phase inversion occur and the dissolved polymer becomes the continuous matrix and the reactive solvent is dispersed as a particulate phase.

This novel processing technique was initiated in our laboratory by Venderbosch *et al.*[7] for processing of poly(2,6 dimethyl-1,4-phenylene ether) (PPE), often referred to as PPO, and different epoxy resins as the reactive solvent. PPE is a typical high T_g (215°C) thermoplastic material which can be considered to be intractable. Processing via the melt is not feasible in view of severe thermal degradation at the high temperatures required for extrusion or injection-moulding, typically $T_g + 100$ K. By dissolving PPE in an epoxy resin, and subsequently curing the epoxy resin/PPE solution in the mould, complete phase separation and phase inversion occurs. The originally dissolved thermoplastic polymer, PPE, becomes the continuous phase and the epoxy resin is dispersed as a particulate thermoset phase in the matrix. Consequently, the properties of the composite structure are dominated by the characteristics of (pure) PPE and by choosing the proper epoxy resin, varying from a low T_g to a high T_g epoxy thermoset epoxy phase after curing, the final properties of the composite structure can be tuned. The PPE/epoxy system can also be used as a matrix material for fibre-reinforced composites. In this case, the epoxy phase can act as the interface between the fibre and matrix[8,9].

Our novel processing route for processing intractable polymers, involving in situ polymerisation of monomers in the presence of polymers is to some extent comparable with the synthesis of interpenetrating polymer networks (IPNs)[10–12], notably the class of semi-IPNs[13–20]. However, in our processing technique employing reactive solvents, no explicit attempts are made to obtain interpenetrating

* To whom correspondence should be addressed

structures. On the contrary, in the case of PPE/epoxy, complete phase separation occurs.

The system PPE/epoxy is just one example of the use of reactive solvents to lower the processing temperature enabling processing of intractable polymers. Many other high T_g polymers, like poly(ether-sulphone) (PES)[21,22], poly(sulphone) (PSU), poly(ether-imide) (PEI) and poly(-ether-ether-ketone) (PEEK) can be interesting materials in this respect[23].

The advantage of using reactive solvents is that both the processing temperature and viscosity can be lowered with respect to the polymer to be processed and, moreover, there is *no need for solvent removal* after processing: the solvent becomes a structural part of the final system and can be even a very useful constituent, depending on the choice of the proper reactive solvent (monomer).

In this respect, the use of a reactive solvent is not limited to intractable polymers, but can also be useful for processing normal standard, i.e. tractable, polymers as well, like polyethylenes, polypropylenes and ethylene–propylene copolymer rubbers (EPR). In our laboratory, we have investigated the application of 'pourable' polyethylenes and rubbers to make complex shaped products. Polyethylene can be dissolved in styrene and the low viscosity solutions can be transferred into a mould and, upon subsequent polymerisation, the dissolved polyethylene becomes the continuous phase, similar to the PPE case discussed before. In the literature, it has already been reported that styrene can be used as a solvent for polyethylene[24–27]. Studies by Borsig *et al.* were aimed at obtaining IPN-like structures[24–26], while the use of styrene as a processing aid for UHMW-PE was patented by Hercules[27]. The basic concept of the latter study was to lower the viscosity of UHMW-PE by processing a heterogeneous suspension of UHMW-PE in styrene at room temperature into a pressurised, heated mould. The suspension was then homogenised in the mould and simultaneously the solvent was polymerised in situ. In contrast with that study, we aim at processing the homogeneous solution ('pourable polyethylenes') and subsequent polymerisation the solvent in situ.

In this study we wish to report the structure development during polymerisation of polyethylene/styrene mixtures with the aim of morphology control in view of the fact that the properties of the final system, PE/PS, are determined mainly by the morphology. Use was made of in situ X-ray studies (SAXS and WAXS), as has been applied in elucidating structure development in several other complex systems[28–30] including studies on reactive systems, e.g. by Ryan and co-workers[31–34]. Simultaneous SAXS/WAXS experiments were performed on the PE/styrene system in order to determine the morphology development, i.e. the kinetics of phase separation and crystallisation combined with Raman spectroscopy studies to follow monomer to polymer conversion.

EXPERIMENTAL

Materials and blend preparation

High-density polyethylene ($M_n = 14$, $M_w = 73$ kg mol^{-1}) was supplied by DSM and used as received. The reactive solvent styrene (Merck) was used without purification. For initiation of the polymerisation, a mixture of dibenzoyl peroxide (Lucidol) and *tert*-butyl peroxybenzoate (Trigonox C), supplied by AKZO, was added for a relatively fast polymerisation. For a slow polymerisation, a mixture of *tert*-butyl peroxybenzoate and dicumylperoxide (Perkadox BC), also from AKZO, was used. For the miscibility study, a small amount of inhibitor (benzoquinone, Aldrich) was added to prevent thermal polymerisation while dissolving PE in styrene.

Solutions of PE in styrene with a content up to 35 wt.% were prepared by dissolving PE in styrene using a mechanical stirrer at a temperature up to 120°C. A stirring time of approximately 15 min was needed to obtain optically homogeneous solutions. Then the initiator mixture was added. PE/styrene solutions at high concentrations (> 35 wt.%) were prepared in a recirculating co-rotating twin-screw mini-extruder (volume of 5 cm^3). The initiators were mixed with styrene at room temperature. Then the PE powder was added to the styrene. In the next step, the suspension was charged into the feeding section of the mini-extruder. Due to efficient mixing, a mixing time of approximately 2 min was sufficient to obtain a homogeneous solution.

Miscibility of PE and styrene

In order to determine the miscibility of styrene and PE, calorimetric observations were performed on a Perkin-Elmer DSC-7 apparatus. Samples with different PE contents were transferred into high-pressure d.s.c. sample pans and subsequently sealed. High-pressure d.s.c. sample pans were used to prevent any volatilisation of styrene. Different heating and cooling rates were used to determine the phase diagram.

To check the possibility of the interference of liquid–liquid (L–L) phase separation with crystallisation, combined calorimetric and optical observations were performed on a modified Perkin-Elmer DSC-7 equipped with a light transmission set-up[35]. The samples were introduced in a modified high-pressure d.s.c. sample pan with a quartz window and a silicon wafer mirror at the bottom of the sample pan and subsequently sealed. Together with the heat flow signal, light transmission data were acquired with a separate detector system.

Morphology

The morphology of the PE/PS blends was examined by transmission electron microscopy, performed on a Jeol JEM 2000 FX transmission microscope, operated at 80 kV. For TEM, fracture surfaces were trimmed and subsequently stained by RuO_4 for 16 h for contrast enhancement between the amorphous and crystalline regions and for morphology fixation. Finally, thin sections were obtained by ultramicrotomy at room temperature using a Reichtert Ultracut E microtome.

Morphology development

To study the morphology development upon in situ polymerisation of styrene, simultaneous time-resolved small-angle X-ray scattering (SAXS) and wide-angle X-ray scattering (WAXS) experiments were performed on Beamline 8.2 of the Synchrotron Radiation Source (SRS) at Daresbury Laboratory, Warrington, UK. Details of the storage ring, radiation, camera geometry, and data collection system are described in Ref. 36.

The WAXS data were collected with a curved Inel detector positioned in such a way that its centre of curvature coincided with the sample position. The SAXS patterns were collected on a multiwire quadrant detector positioned at 3.5 m from the sample. The SAXS and WAXS data were collected simultaneously every 30 s.

PE/styrene solutions were transferred into Lindemann capillaries and subsequently sealed. The capillaries were

placed in a capillary holder fixed on a Linkam THMS 600 hot-stage mounted on the optical bench. The silver heating block of the hot-stage contained a $4 \times 1\ mm^2$ conical hole allowing the X-rays to pass through. In the capillary holder a J-type thermocouple was fitted to measure the approximate temperature.

For calibration of the SAXS detector, the scattering pattern from an oriented specimen of wet collagen (rat-tail tendon) was used. PE single crystals were used to calibrate the WAXS detector. A parallel plate ionisation detector was placed in front of and after the sample to record the incident and transmitted intensity. The experimental data were corrected for background scattering, i.e. subtraction of the scattering from the camera, hot stage, and an empty capillary.

Reaction kinetics

The reaction kinetics was investigated by Raman spectroscopy at the Van der Waals–Zeeman laboratory at the University of Amsterdam. Raman spectra were obtained with a Dilor XY-800 spectrograph coupled with a liquid nitrogen-cooled EG&G Princeton CCD array detector. The 488 nm line of a Spectra-Physics Stabilite 2016 argon ion laser was used as the incident light on the sample, while the spectra were obtained in backscattering mode. The samples were contained in sealed capillaries. The capillaries were placed in a capillary holder fixed on a Linkam THMS 600 hot-stage, which was mounted on an XYZ-table for sample positioning.

RESULTS AND DISCUSSION

Miscibility of polyethylene and styrene

The miscibility of polyethylene and styrene was investigated to explore the temperature–composition area for processing the required homogeneous solutions. The experimental melting (dissolution) and crystallisation curves as a function of composition are shown in *Figure 1*. The crystallisation curve was obtained by cooling the samples in the d.s.c. apparatus. Upon cooling, an exotherm is observed due to crystallisation and the onset of this exotherm, extrapolated to zero scan rate, was taken to construct the crystallisation curve shown in *Figure 1*. Upon heating the crystallised samples, an endotherm is observed related to melting (dissolution) of the crystals and the tail of the endotherm, intersecting the base line, and extrapolated to zero scan rate, was taken as the melting temperature, i.e.

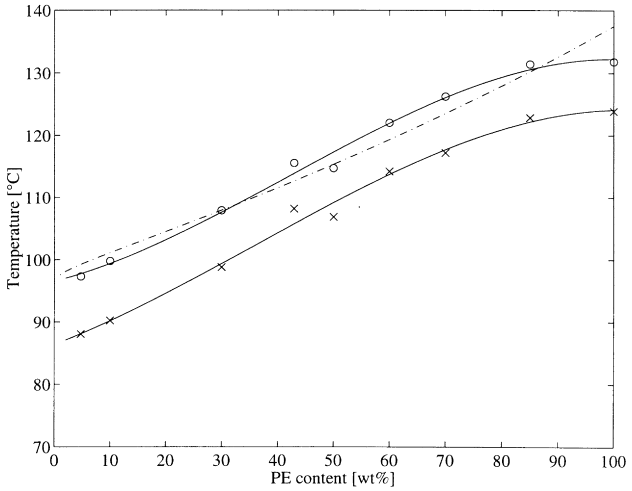

Figure 1 Phase diagram of PE–styrene solutions: (×) crystallisation; (○) melting; (—) calculated melting temperature depression

the temperature at which the last crystals dissolve in the solution.

Experimental melting c.q. dissolution curves are commonly analysed using the well-known melting–depression relationship based on the Flory–Huggins lattice theory which reads for high molar mass polymers:

$$\frac{1}{T_m} - \frac{1}{T_m^0} = \frac{RV_2}{\Delta H_m V_1}[\phi_1 - \chi\phi_1^2] \quad (1)$$

In equation (1), T_m is the melting (dissolution) temperature as a function of the composition and T_m^0 is the equilibrium melting temperature of the pure polymer, ΔH_m the melting enthalpy per monomer unit, and ϕ_1 the solvent volume fraction. V_1 and V_2 represent the molar volume of the solvent and the polymer, respectively. The interaction parameter χ can be expressed, using the Hildebrandt solubility parameters of the solvent, δ_1, and the polymer, δ_2, as

$$\chi = \frac{V_1(\delta_1 - \delta_2)^2)}{RT} \quad (2)$$

The calculated equilibrium melting temperature as a function of composition is also plotted in *Figure 1*, using literature values for the parameters as listed in *Table 1*[37,38]. In calculating the melting temperature as a function of the composition, a value of 410.6 K was taken for the equilibrium melting temperature of polyethylene in order to fit the calculated curve to the experimentally determined dissolution curve. The authors are aware of the fact that the equilibrium melting point T_m^0 of polyethylene is 419 K, but taking this value implies simply a shift in the curve upwards. We merely want to demonstrate here that polyethylene in styrene above the experimental curve of T_m *versus* ϕ is a homogeneous solution. There is no indication for an interference with a L–L demixing, as reported by Richards[39], Roginova and Slonimskii[40] and Nakajima *et al.*[41] for several PE–solvent systems. This was substantiated by additional combined calorimetric and light-transmission measurements. In conclusion, styrene is a good solvent for PE at elevated temperatures.

Morphology as revealed by TEM

Upon (isothermal) polymerisation of styrene phase separation will inevitably occur, since PS is immiscible with PE. Some representative TEM micrographs of PE/PS blends, resulting from this chemically induced phase separation, are presented in *Figure 2a–d*. The micrographs clearly show a phase-separated and phase-inverted morphology of dispersed PS particles in a matrix of PE. Previous results[42] showed that phase inversion can already occur at a PE content between 5 and 10 wt.%. The influence of the blend composition on the morphology is also evident. An increase in PE content results in a decrease in PS particle diameter, probably related to kinetic constraints on the coarsening process, due to an increase in viscosity. The importance of coarsening is also evident from the morphologies presented in *Figure 2c,d*.

The PE lamellae are embedded between PS particles. For the low PE contents, only one or two lamellae are observed between the repeating PS particles.

Table 1 Constants for the calculation of melting temperature depression

	T_m^0 (°C)	V_2 ($cm^3\ mol^{-1}$)	ΔH_m (kJ/mol, $-CH_2-$)	δ_H ($MPa^{1/2}$)
Styrene	−30.8	115.6	—	19.0
PE	137.6	32.8	7.9	17.0

Morphology development as revealed by SAXS and WAXS

In situ SAXS and WAXS data were simultaneously collected during isothermal polymerisation. Two temperatures were selected for the present experiments: 120 and 125°C. At the polymerisation temperature, T_p, of 125°C, no phase crystallisation is to be expected, see also the phase diagram in *Figure 1*, since T_p is always above the experimentally determined crystallisation curve and only a chemically induced (L–L) demixing can occur. At the polymerisation temperature of 120°C, crystallisation can occur at a later stage of the polymerisation process when the dissolution temperature of PE in residual styrene exceeds T_p, see also *Figure 1*.

Figure 3 shows the recorded SAXS and WAXS data. The SAXS data are presented as three-dimensional plots of intensity, $I(q)$, *versus* scattering vector, $q = (4\pi/\lambda) \sin \theta$, where 2θ is the scattering angle, as a function of the polymerisation time. The WAXS data are only given for the polymerisation temperature of 120°C in *Figure 3b,d* as three-dimensional plots of intensity, $I(2\theta)$, *versus* scattering angle 2θ, *versus* time. All SAXS patterns (*Figure 3a,c,e,f*) show initially little scattering intensity indicative of homogeneous solutions as is to be expected from the phase diagram in *Figure 1*. During polymerisation, the scattering patterns all gradually change. At the polymerisation temperature of 120°C, a different WAXS pattern is observed at the later stage of the polymerisation process showing the characteristic 110 and 200 reflections and the reflections of the higher orders of the orthorhombic unit cell (see *Figure 3b,d*). No WAXS pattern is observed at 125°C as explained above.

First we wish to focus on the SAXS and WAXS patterns obtained at 120°C (*Figure 3a–d*). Before crystallisation sets in, the intensity of the SAXS patterns increases which is

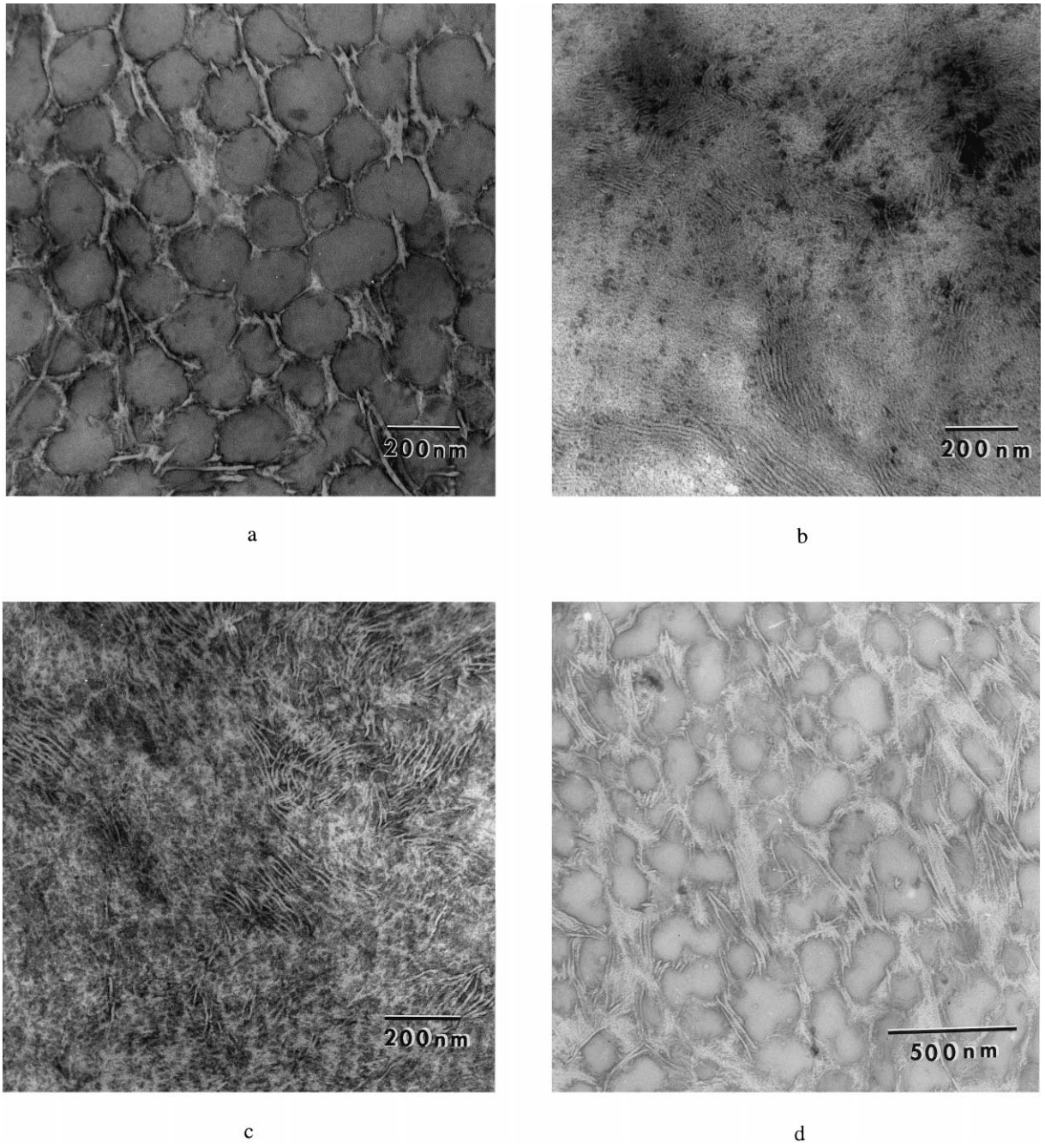

Figure 2 TEM micrographs of PE/PS blends with a PE content of (a) 20 wt.% PE; (b) 60 wt.% PE, polymerised at 120°C (fast initiator mixture); (c) 60 wt.% PE, polymerised at 125°C; and (d) 60 wt.% PE, polymerised at 120°C (slow initiator mixture)

related to the chemically induced phase separation process. When crystallisation starts, the intensity of the SAXS patterns decreases and a broad shoulder appears in the q range of 0.01–0.03, which intensifies on further polymerisation until no changes are observed, hence the morphology is fixed.

There is, however, a noticeable difference between the phase separation processes, before crystallisation, for the two concentrations, respectively, 20 and 60 wt.%. In the case of the 20 wt.% PE solution, the intensity *versus* the scattering vector q, decays monotonically and no (local) maximum is observed. Upon plotting the intensity *versus* time t^2, the typical t^2 dependence is observed (see *Figure 4*), which is indicative of a phase separation process involving nucleation and growth as discussed by Lipatov *et al.*[43]. In the case of the 60 wt.% solution, a local maximum is observed indicative of a periodic microstructure in the order of 400 Å, as calculated from Bragg's law, before crystallisation sets in. This periodic microstructure could be indicative for a spinodal type of phase separation process. According to the (linearised) Cahn–Hilliard theory[44], concentration fluctuations with a dominant wave number will grow giving rise to a periodic microstructure.

Up to now, only qualitative explanations have been proposed to explain the observed phenomena. However, additional information can be obtained by a more detailed analysis of the data combined with a proposed model (see below).

Analysis of SAXS and WAXS data

The growth of the scattered intensity can be related to electron density fluctuations. The degree of phase separation

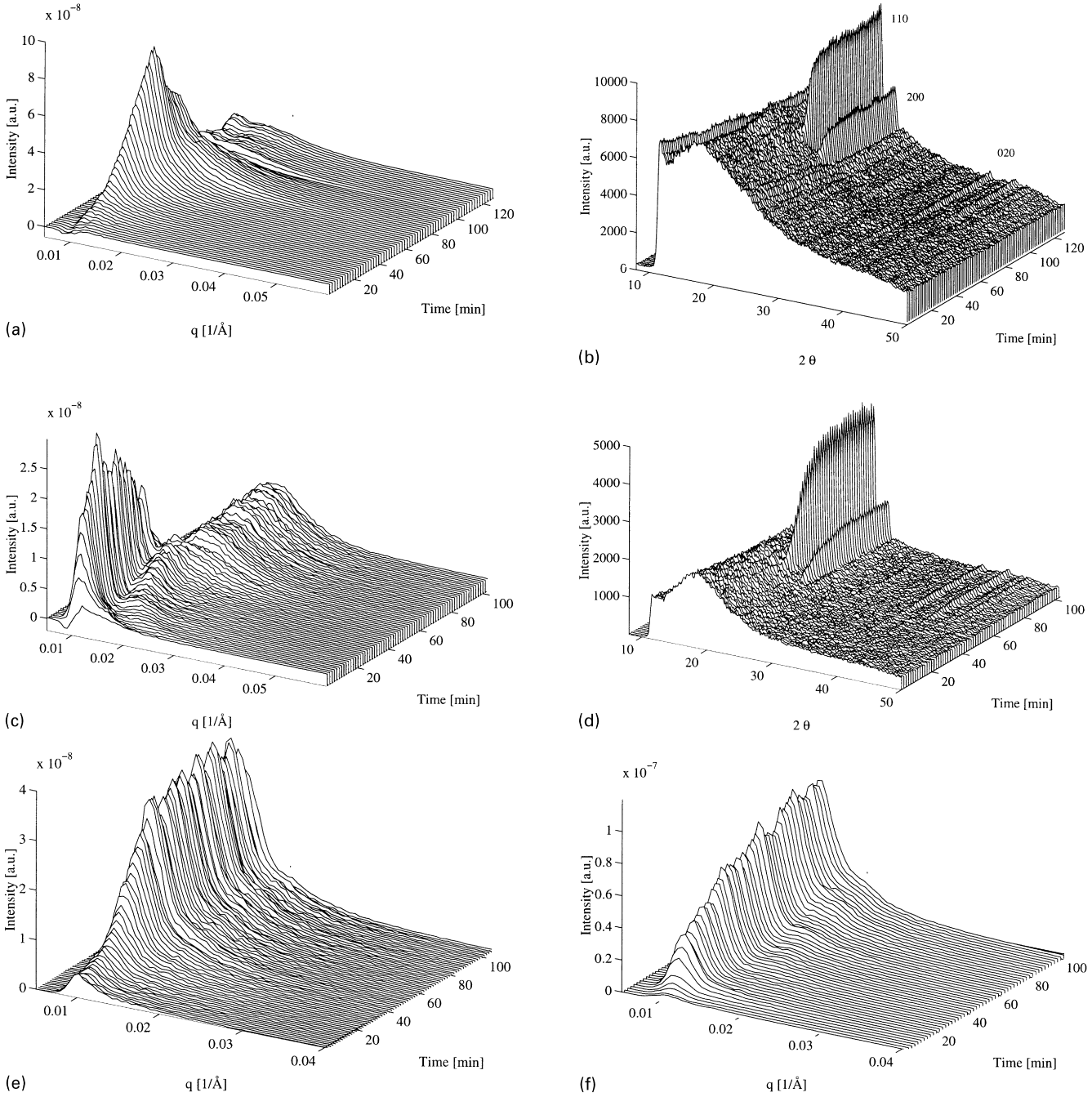

Figure 3 (a) SAXS data for the polymerisation temperature of 120°C of 20 wt.% PE. Intensity, $I(q)$, *versus* scattering vector q, *versus* time. (b) WAXS data for the polymerisation temperature of 120°C of 20 wt% PE. Intensity, $I(2\theta)$, *versus* scattering angle, 2θ, *versus* time. (c) As (a), 120°C, 60 wt.% PE. (d) As (b), 120°C, 60 wt.% PE. (e) As (a), 125°C, 20 wt.% PE. (f) As (a), 125°C, 60 wt.% PE

Table 2 Densities and electron densities for the individual components[45]

Component	Density (g cm^{-3})	Electron density (mol electrons cm^{-3})
Styrene	0.909	0.489
PS	1.05	0.565
Amorphous PE	0.855	0.489
Crystalline PE	1.014	0.580

can be related to these electron density fluctuations. For a two-phase system with sharp boundaries, the mean-square electron density fluctuation is defined by

$$\langle \eta^2 \rangle = \phi_1 \phi_2 (\rho_1 - \rho_2)^2 \tag{3}$$

where ϕ_i denotes the volume fractions and ρ_i the electron densities of the components. The electron densities of the individual components are listed in *Table 2*. The mean-square electron density fluctuation can be calculated from the experiments:

$$\langle \eta^2 \rangle = \frac{Q}{2\pi i_e} = \frac{1}{2\pi i_e} \int_0^\infty I(q) q^2 \, dq \tag{4}$$

where Q is the invariant, independent of the topology or geometry of the scattering units and i_e is the Thompson scattering constant for a free electron. The use of the invariant as a function of time is useful to evaluate the structural changes during polymerisation and additional information may be obtained. The calculation of the absolute value of the invariant requires absolute intensity measurements, correction for thermal fluctuations, and for the integration from $q = 0 \rightarrow \infty$, extrapolation to $q \rightarrow 0$ and ∞. Because of experimental constraints, the experimental invariant is calculated by integrating from the first to the last reliable data point[46]. In *Figure 5* the experimental invariants for the 20 and 60 wt.% PE systems at the two polymerisation temperatures (120 and 125°C) are presented.

For the 20 wt.% PE systems, a maximum for the experimental invariant is found in the early stages of the L–L phase separation. Because the electron density contrast, $(\rho_1 - \rho_2)$, between the PE-rich and PS-rich regions only increases during the polymerisation, the maximum must be attributed to changes in the volume fractions of the two phases. The volume fraction of the PE-rich phase ranges from 1.0 before the onset of L–L phase separation to an end value of 0.2. The invariant reaches a maximum close to equal phase volumes. The difference in time to reach this maximum for the two polymerisation temperatures reflects the influence of temperature on the reaction rate. On further polymerisation, a plateau is found for the system polymerised at 125°C, indicating that no further structural changes occur. For the polymerisation at 120°C, a second maximum in the invariant is observed. This originates from crystallisation of PE. Upon crystallisation the system becomes a three-phase system. Assuming sharp phase boundaries, the mean-square electron density fluctuation is then expressed as

$$\langle \eta^2 \rangle = \phi_1 \phi_2 (\rho_1 - \rho_2)^2 + \phi_1 \phi_3 (\rho_1 - \rho_3)^2 + \phi_2 \phi_3 (\rho_2 - \rho_3)^2 \tag{5}$$

where ρ_1 represents the amorphous PE-rich phase, ρ_2 the PS-rich phase and ρ_3 denotes the crystalline PE phase. The major contribution to the change in the invariant is found in the second term of equation (5), $\phi_1 \phi_3 (\rho_1 - \rho_3)^2$, although the occurrence of a maximum cannot be ascribed to the second term alone, since both, the change in volume fractions of the individual phases as well as the electron density contrast values, are unknown.

The experimental invariants of the 60 wt.% PE systems do not show a maximum, because the phase volumes do not become equal. The invariant measured for the polymerisation at 125°C increases with time. Two regions can be distinguished. Initially a sharp increase is observed, followed by a more gradual increase. The development of the invariant in the first region is, most likely, dominated by the change in phase volumes. The change in slope might indicate that no major phase volume changes take place and that the increase must be due to further enhancement of the electron density contrast. Similar to the 20 wt.% PE system, the onset of the crystallisation results in an increase of the invariant, although this increase is much smaller than for the 20 wt.% PE system.

As already shown in *Figure 3b,d*, crystallisation can set in during the isothermal polymerisation. The crystallisation rate, which can be derived from the intensity of the 110 and 200 reflections, is dependent on the PE content, as can be

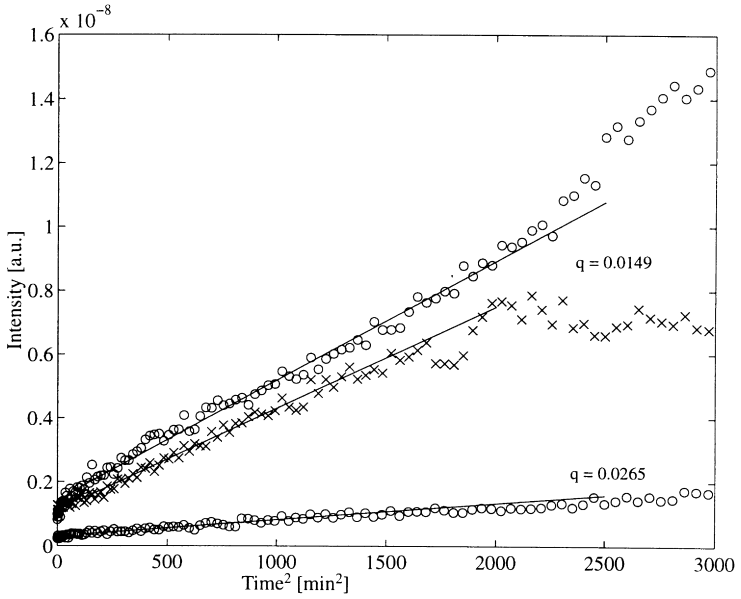

Figure 4 Intensity, $I(q)$, *versus* time squared for 20 wt.% PE: polymerisation temperature, 120°C (×), 125°C (○)

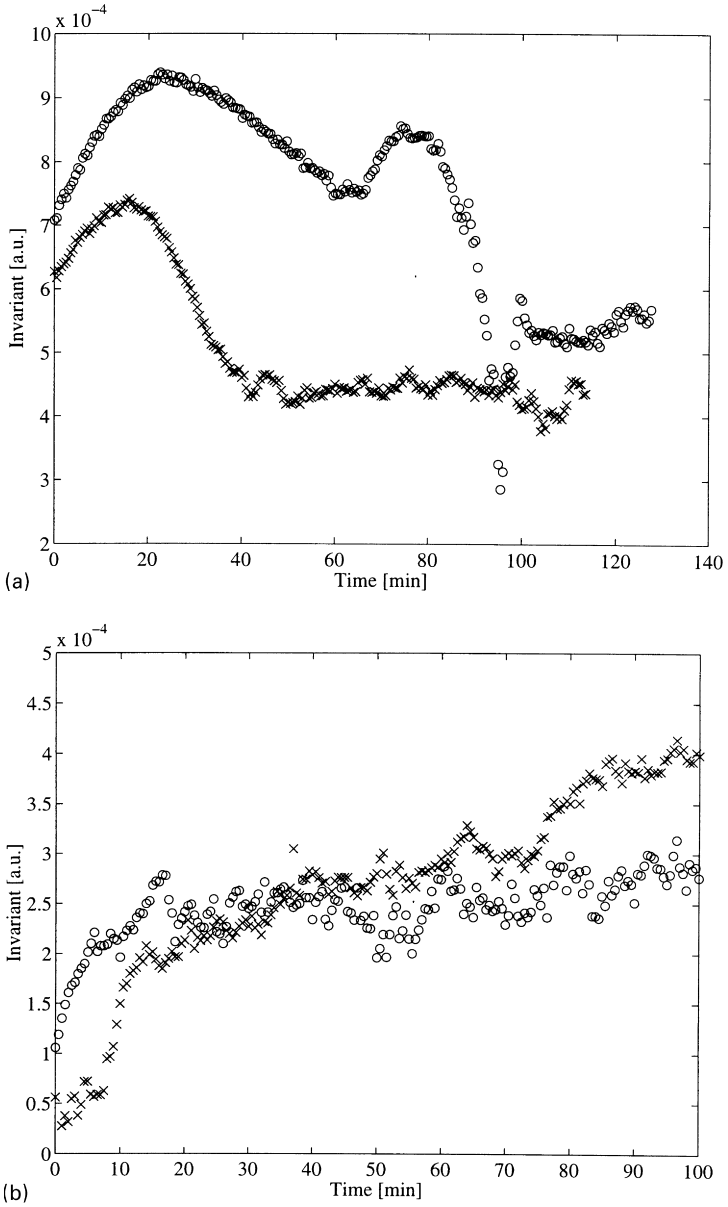

Figure 5 The experimental invariants for (a) 20 wt.% PE polymerised at 120°C (○) and 125°C (×) and (b) 60 wt.% PE polymerised at 120°C (○) and 125°C (×)

seen in *Figure 6*. For the 60 wt.% PE system, the crystallisation rate is much slower. Upon crystallisation, the solvent is expelled from the PE-rich domains. The rate of diffusion of solvent has a great influence on the crystallisation rate. For higher PE contents, the PE-rich domains are much larger in size resulting in larger diffusion lengths. Accordingly, the expulsion of the solvent is slower. The absolute degree of crystallinity cannot be derived from these results, because the halo from amorphous PE partially overlaps with the diffuse halo of both styrene and PS, originating from the correlation between the phenyl groups[47].

Upon polymerisation of styrene in the homogeneous PE solutions, a third component is formed: PS. It is important to note that the system is not in equilibrium due to the continuous formation of polystyrene chains and, moreover, that we are dealing with multi-component systems. Nevertheless, to get a fundamental insight into the system and to explain the several transitions occurring, the use of a simple (equilibrium) ternary phase diagram, as shown in *Figure 7*, might be useful for the present discussion on the morphology development.

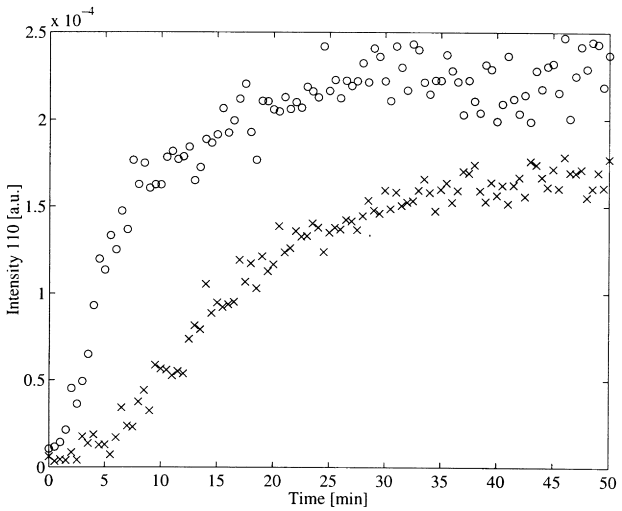

Figure 6 Crystallisation rates for 20 wt.% PE (○) and 60 wt.% PE (×) during polymerisation at 120°C

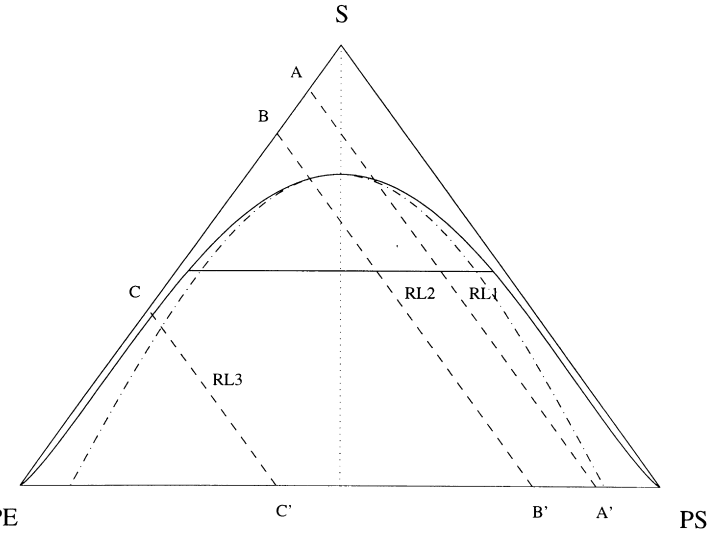

Figure 7 Schematic ternary phase diagram for PE/PS/styrene. For details, see text

The initial composition of the homogeneous solution is located on the PE–styrene axis. The polymerisation takes place at a fixed temperature, T_p. Upon polymerisation a reaction line is followed as indicated by the dashed lines in *Figure 7*. After little conversion of styrene, the binodal line (solid line) is crossed and the system becomes metastable, eventually leading to phase separation in a two-phase system with one phase rich in PS and the other phase rich in PE. The position of the binodal and spinodal curves depend on the molecular weights of the two polymers and the interaction parameters between the polymers and the solvent. Considering the case that the interaction between the solvent and both polymers are identical, the critical point is located at the maximum of the binodal and the corresponding tie lines are horizontal, when the polymers have equal molecular weights.

To explain the different morphologies that can be obtained, several reaction lines can be considered in *Figure 7*. When the initial composition is located in the interval to the right of the critical point (A–A′ in *Figure 7*), phase separation results in a two-phase system of a dispersed phase rich in PE and a matrix phase rich in PS. When the initial composition is located in the interval to the left of the critical point, the dispersed phase is rich in PS and the matrix phase is rich in PE, as for instance reaction lines B–B′ or C–C′. The composition of the phases consists of polymer in solvent, where the other polymer is only present in a very small quantity. In that respect, the assumption that no PS is present in the PE-rich phase may be justified. For systems with a low initial polymer concentration, the reaction line can cross the line of equal volume fractions. The maximum observed in the invariant (see *Figure 6a*) is related to this cross-point (see equation (3)).

For a given initial concentration, i.e. considering only one reaction line, the morphology can be altered by influencing the reaction rate relative to the rate of phase separation. When the binodal line is crossed the system becomes metastable and phase separation is induced. Depending on the location of the spinodal (dash/dotted line) and the relative rates of polymerisation and phase separation, the demixing can take place via a nucleation and growth mechanism, via a gradual transition from demixing via nucleation and growth to spinodal demixing, or the system is immediately thrust into spinodal demixing, all resulting in two-phase systems, but with completely different morphologies. For the systems studied, this can be established by changing the thermal stability of the initiators, when the polymerisation temperature is kept constant. The resulting change in morphology is evident from the TEM micrographs (*Figure 2b,d*).

Now, we focus on the PE-rich phase, which plays a decisive role in the resulting mechanical properties. With ongoing polymerisation, the PE content increases, because styrene and PS, just formed, diffuse to the PS-rich phase to attain equilibrium conditions. The diffusion of styrene and PS out of the PE-rich domains is hampered by the increasing viscosity. The constraints on the diffusion become more important for higher PE contents, since in that case the PE-rich domains are larger, resulting in larger diffusion lengths. When polymerised below the crystallisation temperature of the neat PE, the PE content in the PE-rich phase can reach such a level, that the degree of undercooling is sufficiently high. This induces a liquid–solid (L–S) transition, i.e. crystallisation as schematically drawn in *Figure 8*. The remaining solvent then will be expelled from the crystalline regions.

The PE content at which the L–S transition occurs only depends on the temperature and not on the initial composition. The morphology of the PE crystalline regions therefore only depends on the polymerisation temperature. It must be stressed, however, that the sizes of the PE

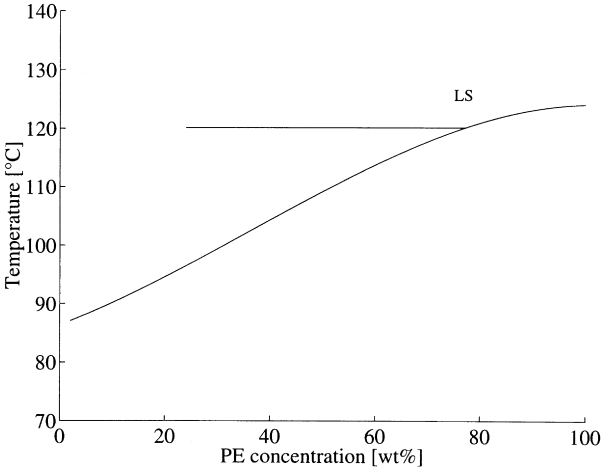

Figure 8 Schematic representation of the L–S transition in the PE-rich phase

domains play an important role in the diffusion of styrene monomer and PS chains. When styrene or PS is locked in the PE, upon crystallisation, this may lead to a lower degree of crystallinity or PS chains may get trapped in the amorphous regions, especially for the higher initial PE contents.

The former discussion with the help of ternary phase diagram and the time evolution of the invariant, directly related to electron density fluctuations $\langle \eta^2 \rangle$, and thus degree of phase separation, can be used to explain the development of the SAXS patterns. First, we consider the low-PE content solutions, i.e. 20 wt.% PE. In the initial stages of the polymerisation, the PE/styrene solution is homogeneous. Thus, the value of $\langle \eta^2 \rangle$ will be equal to zero. This is represented by the straight line in the first plot in *Figure 9*. The second plot shows the electron density profiles upon L–L phase separation via the nucleation and growth mechanism. The PS-rich phase has a higher electron density than the PE-rich phase. The dashed lines represent the progress of the electron density profiles as a function of time. The electron density difference between the two phases increases as the PS-rich phase becomes richer in PS with a high electron density ($\rho_S = 0.565$ mol e$^-$ cm^{-3}), whereas the PE-rich phase becomes richer in amorphous PE with a low electron density ($\rho_{aPE} = 0.489$). The growth of the domains is indicated by the increasing size of the different profiles.

When the L–S transition sets in, a major change in the PE-rich domains occurs as represented in plot 3. As the crystalline PE has a higher electron density than the amorphous PE, electron density fluctuations on much smaller scale develop. The remaining styrene monomer, still present in the PE-rich phase, diffuses either to the amorphous PE regions or forms new domains, having a different electron density compared to the other components. Plot 4 in *Figure 9* represents a final electron density profile.

For the 60 wt.% PE system, the electron density profiles should be different, because the sizes of the regions are dependent on the concentration. The first profile is similar, although the absolute value of the electron density is lower (see *Figure 10*). Because the polymerisation rate is much higher, the profile becomes dissimilar from the low-PE content profile as the L–L phase separation changes from a nucleation and growth mechanism to spinodal decomposition This is represented by the second plot in *Figure 10*. It shows the increase in contrast (solid lines) as well as the coarsening of the structure (dotted lines). Upon further polymerisation and phase separation the phase boundaries may also become sharper. This is indicated in plot 3. When the L–S transition sets in, similar changes in the profile as for the low-PE content profiles can be drawn. Plot 4 in *Figure 10* represents a final electron density profile.

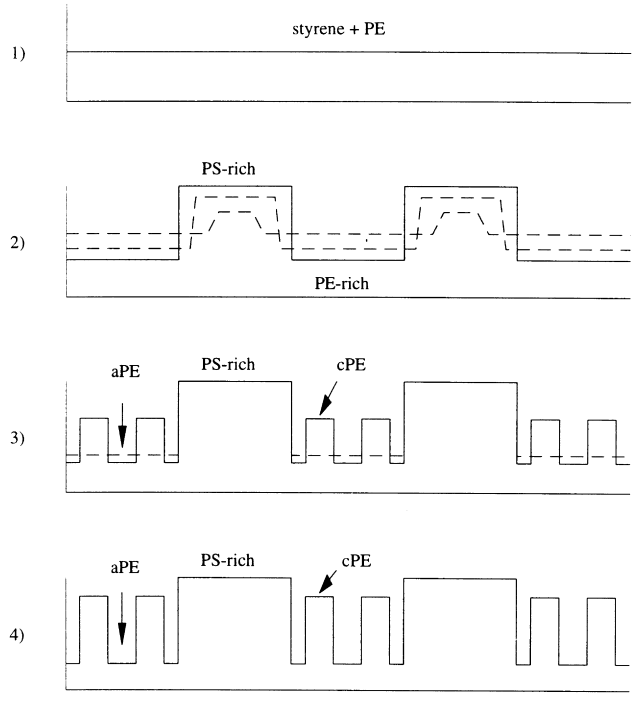

Figure 9 Schematic electron density fluctuation profiles for the 20 wt.% PE blends

Reaction kinetics

The polymerisation reaction of styrene and other vinyl monomers can be monitored by the C=C stretching vibration band at ~1631 cm^{-1}. The intensity of this band decreases as polymerisation proceeds, and the magnitude relative to either the initial peak intensity or to an internal reference peak, that does not change during polymerisation, yields information about conversion as a function of time. Chu and co-workers[48,49] and Sears *et al.*[50] already investigated styrene bulk polymerisation by Raman spectroscopy. Both studies emphasised the need for an internal reference and used the ring breathing mode of the phenyl group at 1000 cm^{-1}. The shift of this strong, sharp peak is only 2 cm^{-1} from styrene to PS. The intensity ratio of the polymer to monomer, however, changes. Sears *et al.* reported a ratio of 0.42, but their data show large scatter. Chu and co-workers measured a ratio of 0.59. These results were obtained by preparing polymer–monomer mixtures of different concentrations, but these mixtures were measured at room temperature, while Gulari *et al.*[51] reported different ratios, dependent on temperature. In conclusion, these significantly different results show that the use of the breathing mode of the phenyl group as internal reference has some limitations. Gulari *et al.* emphasised that it is better to use the absolute peak areas to measure the conversion quantitatively. In contrast with the above-reported results, we did not observe a significant change of the integrated peak area for styrene bulk polymerisation at 120°C. One important remark that has to be made, especially for our systems, is the condition that the sample should not become turbid or develop air bubbles in the scattering volume.

For styrene, the 621 cm^{-1} peak, characteristic for the mono-substituted phenyl group, can also be used as an internal reference. For styrene it is known that the ratio of

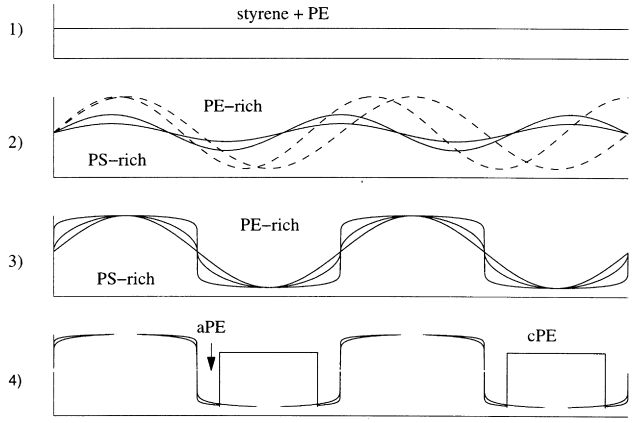

Figure 10 As *Figure 9*, now for the 60 wt.% PE blends

the integrated intensities of the 621 and the 1631 cm^{-1} bands is equal to 27[52]. Because a linear correlation is found between the intensity ratio and the amount of double bonds, this ratio can be used to calculate the double bond content, and thus conversion. Because we are only interested in the effect of PE concentration and polymerisation temperature on the styrene conversion, and not in absolute degrees of conversion, a simplified equation for conversion, $X(t)$, is used:

$$X(t) = 1 - \left(\frac{I_{1631}(t)}{I_{621}(t)} \Big/ \frac{I_{1631}(0)}{I_{621}(0)} \right) \quad (6)$$

In a similar way, the degree of crystallisation can be monitored as a function of time. A comparison of results on neat PE showed good agreement with degrees of crystallinity derived from density, SAXS and WAXS measurements[53]. These results of Strobl and Hagedorn showed that the Raman spectrum of partially crystalline PE can be described as a superposition of three components, originating from the orthorhombic crystalline phase, a melt-like amorphous phase, and a transition layer, i.e. a disordered, anisotropic phase. From the integrated intensities of the characteristic bands, the mass fraction of the individual phases, and thus the degree of crystallinity, could be derived. More details together with the assignment of the PE-peaks are given in Ref. [53].

A prerequisite to calculate the degree of crystallinity for our systems is, of course, that there is no overlap of peaks originating from PE, PS, and styrene. *Figure 11* shows the Raman spectra of the individual components. The spectra are normalised to one, using the maximum intensity of the strongest peak, for scaling purposes.

From *Figure 11*, it is obvious that calculation of the degree of crystallinity is not straightforward for the PE–styrene systems, since there is overlap of peaks in the region between 1250 and 1450 cm^{-1}. In this respect, it must also be remarked that styrene and PS are much stronger Raman scatterers than PE. Therefore, the peaks originating from PE can only be used as an identification tool for the onset of crystallisation.

Figure 12 shows several Raman spectra of the 20 wt.% PE system obtained during in situ polymerisation at 120°C. The data of this system are presented in the form of a three-dimensional plot of intensity *versus* wavenumber and polymerisation time as an example to show the dominant features occurring during in situ polymerisation. First, it is observed that the intensity of the carbon–carbon double bond (C=C) at 1631 cm^{-1} is decreasing with polymerisation time. A second observation is the decrease of the total scattered intensity in the early stage of the polymerisation over the whole wavenumber range. Because the intensity of the incident light can be presumed constant, the decrease must be originating from the change in intensity of the scattered light. This points to the onset of turbidity, resulting from phase separation. The occurrence of phase separation after short polymerisation times was also evident from the SAXS-patterns. With Raman spectroscopy, however, it is possible to quantify the styrene conversion needed to induce L–L phase separation. A third feature, that can be seen from *Figure 12*, is crystallisation of PE. Similar to the WAXS patterns, where the reflections from the PE unit cell appear when crystallisation takes place, Raman peaks are observed in the region between 1050 and 1450 cm^{-1}. The effect of L–L phase separation and the onset of crystallisation on the scattered intensity is even more pronounced when the intensity from a reference peak of styrene is plotted. This is shown in *Figure 13*.

Polymerisation of styrene in bulk is characterised by the presence of three distinct stages regarding the monomer conversion rate. In the first stage, the reaction mixture has a

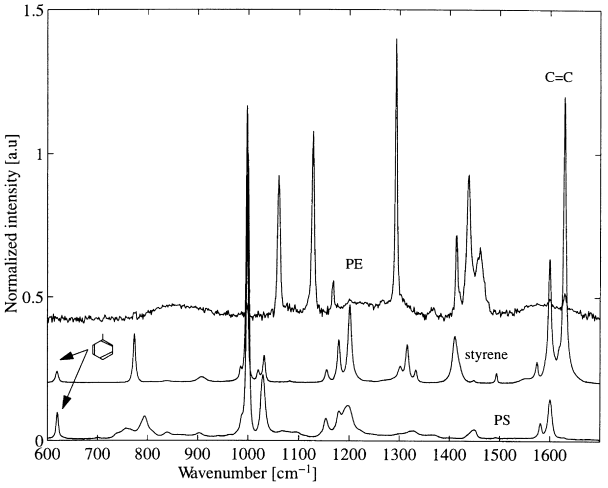

Figure 11 Raman spectra for styrene, PS, and PE

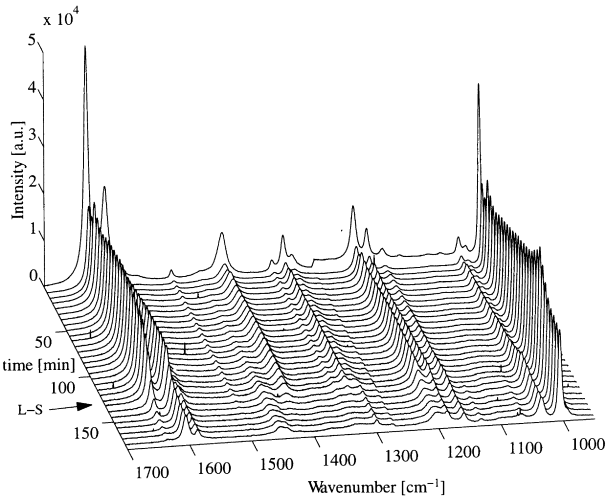

Figure 12 Raman spectra for the polymerisation temperature of 120°C of the 20 wt.% PE system as three-dimensional plot of intensity *versus* wavenumber *versus* time

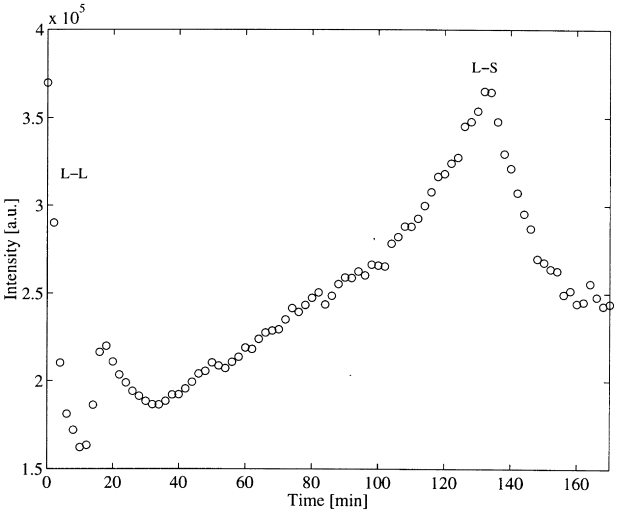

Figure 13 Intensity of styrene reference peak (wavelength 1000 cm^{-1}) as function of time for the 20 wt.% PE system polymerised at 120°C

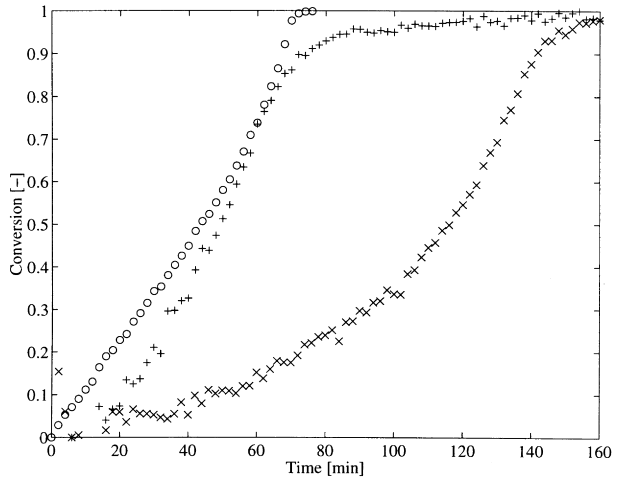

Figure 14 Conversion *versus* time plot, calculated from the Raman spectra: PE–styrene systems polymerised at 120°C: (×) 20 wt.% PE, (+) 60 wt.% PE, and styrene bulk polymerisation (○)

low viscosity. The propagation rate and the rate of termination (for styrene it is known that termination occurs mainly by recombination) are high. At a certain point, the termination reaction will become diffusion controlled, because the viscosity of the reaction mixture increases. The propagation reaction is not much influenced in this stage. The radicals mainly react with monomer, forming new radicals. This leads to an increase of the overall polymerisation rate. This is called the auto-acceleration or Tromsdorff effect. At higher conversion, the overall reaction rate decreases, because the propagation reaction becomes also diffusion controlled, and because of depletion of monomer.

The time evolution of the styrene conversion for the 20 and 60 wt.% PE systems, polymerised at 120°C, are given in *Figure 14*. For comparison, the time evolution of styrene, polymerised in bulk, is also given. The three stages also appear when styrene is polymerised as a reactive solvent for PE, but the times for the distinct stages will be different. The reason may be two-fold. First, the initial viscosity is higher and depends on the amount of PE. The diffusion of radicals is hampered in an earlier stage of the reaction, leading to initially lower propagation and termination rates, but also the occurrence of the Tromsdorff effect is shifted to shorter times. Secondly, phase separation might also influence the reaction kinetics. It is also observed that the reaction rate is much higher for the 60 wt.% PE systems, although the initiator concentration was kept constant relative to the styrene monomer content. The addition of PE, leading to an increase in viscosity, most probably influences the termination reaction to a greater extent than the propagation reaction. This might also have an effect on the molecular weight of PS. The interference of crystallisation during the polymerisation does not seem to influence the reaction kinetics. Crystallisation can thus be used to stop coarsening of the structure and fix the morphology. This in contrast to fixation of the morphology by vitrification, which slows down the reaction drastically.

CONCLUSIONS

In this study, the principle of processing using reactive solvents was adopted on a standard tractable polymer PE in order to extend the processing characteristics. The use of styrene as a reactive solvent for PE resulted in a significant decrease in both processing temperature and viscosity. Upon in situ polymerisation of styrene, phase separation and phase inversion occurred in the wide composition range studied (10–60 wt.% PE), PE becoming the continuous phase.

First the miscibility was studied. At elevated temperatures a homogeneous solution could be obtained. The system PE–styrene showed no L–L phase separation before crystallisation upon cooling, indicating that styrene is a good solvent for PE.

As revealed by simultaneous SAXS/WAXS experiments and Raman spectroscopy, L–L phase separation occurred in the early stages of the polymerisation reaction, resulting in domains rich in PE and domains rich in PS. Due to the incompatibility of the two polymers, each polymer-rich phase mainly constitutes its own polymer in styrene. When the isothermal polymerisation temperature was below the crystallisation temperature of PE, L–L phase separation was followed by a L–S transition in the PE-rich domains. Upon crystallisation, the solvent is expelled from the PE-rich domains. The rate of diffusion of solvent has a great influence on the crystallisation rate. For higher PE contents, the PE-rich domains are much larger in size resulting in larger diffusion lengths. Accordingly, the expulsion of the solvent is slower. The evolution of the scattering patterns was explained in terms of electron density fluctuation profiles.

The reaction kinetics was followed by Raman spectroscopy. The addition of PE increases the viscosity of the system, affecting both the propagation and termination reaction. For low PE concentrations, this effectively results in a lower overall reaction rate compared to bulk polymerisation of styrene, while for highly concentrated PE systems the reaction rate is comparable.

The morphology of the PE–PS blend, obtained via in situ polymerisation, is the result of chemically induced L–L phase separation and is mainly dominated by the PE content. The reaction rate, however, can also have a significant influence on the morphology, as the L–L phase separation mechanism can be altered from nucleation and growth to spinodal decomposition. When the polymerisation temperature is above the crystallisation temperature of the PE, coarsening of the structure is very slow. The occurrence of the L–S transition during the polymerisation even stops coarsening. Thus, fixation of the morphology can be established by inducing the L–S transition either during polymerisation or upon cooling after polymerisation. L–L phase separation followed by a L–S transition has been reported by Inaba *et al.*[54,55] as a powerful tool to control the morphology in binary mixture of PP and EPR. Fixation of the morphology, induced by the L–S transition, does not have a major influence on the reaction kinetics in contrast with fixation by vitrification[56]. The mechanical properties of the PE–PS blends will be the subject of a subsequent paper, in which also the choice of an alternative reactive solvent, enabling control over the properties of the dispersed phase, will be discussed.

ACKNOWLEDGEMENTS

This research is financially supported by DSM Research (Geleen, The Netherlands). J.G.P. Goossens and S. Rastogi are indebted to the Netherlands Organisation for Scientific Research (NWO) for research and travel grants. The authors would like to thank W. Bras and A.J. Ryan for the assistance in the synchrotron experiments and for the fruitful discussions on the interpretation of the data. Additionally,

the authors like to thank A. Spoelstra for performing the TEM work. J. Schouten is acknowledged for making available the Raman spectroscopy facilities of the Van der Waals–Zeeman laboratory at the University of Amsterdam. The help of W. Koster during the Raman experiments is highly appreciated. Finally, the authors want to thank F. Touwslager and H. Kloosterboer of Philips Research Laboratories for the use of the combined d.s.c.–light transmission equipment.

REFERENCES

1. Kwon, J. D., Kavesh, S. and Prevorsek, D. C., European Applications, 1984, 105169.
2. Kobashi, T. and Takao, S., US Patent 4344908.
3. Smith, P. and Lemstra, P.J., *J. Mater. Sci.*, 1980, **15**, 505.
4. Lemstra, P. J., Kirschbaum, R., Ohta, T. and Yasuda H., *Developments in Oriented Polymers-2*, Chapter 2, ed. I. M. Ward. Elsevier Appl. Science, Oxford, 1985.
5. Chung, C.I., *J. Appl. Polym. Sci.*, 1986, **31**, 2739.
6. Chung, C.I., Cao, M.Y., Liu, C. and Min, K.J., *J. Appl. Polym. Sci.*, 1989, **37**, 1339.
7. Venderbosch, R.W., Meijer, H.E.H. and Lemstra, P.J., *Makromol. Chem. Makromol. Symp.*, 1994, **75**, 73.
8. Venderbosch, R.W., Meijer, H.E.H. and Lemstra, P.J., *Polymer*, 1994, **35**, 4349.
9. Venderbosch, R.W., Meijer, H.E.H. and Lemstra, P.J., *Polymer*, 1995, **36**, 1167.
10. Sperling, L. H., *Interpenetrating Polymer Networks and Related Materials*. Plenum Press, New York, 1981.
11. Huelck, V., Thomas, D.A. and Sperling, L.H., *Macromolecules*, 1972, **5**, 340.
12. Donatelli, A.A., Sperling, L.H. and Thomas, D.A., *Macromolecules*, 1976, **9**, 671.
13. Kim, S.C., Klempner, D., Frisch, K.C., Radigan, W. and Frisch, H.L., *Macromolecules*, 1976, **9**, 258.
14. Devia, N., Manson, J.A., Sperling, L.H. and Conde, A., *Macromolecules*, 1979, **12**, 360.
15. Gergen, W.P., *Kautschuk Gummi*, 1984, **37**(4), 284.
16. Siegfried, D.L., Thomas, D.A. and Sperling, L.H., *J. Appl. Polym. Sci.*, 1981, **26**, 141.
17. Hourston, D.J. and Zia, Y.J., *Appl. Polym. Sci.*, 1983, **28**, 2139.
18. Hourston, D.J. and Zia, Y., *J. Appl. Polym. Sci.*, 1983, **28**, 2745.
19. Hourston, D.J. and Zia, Y., *J. Appl. Polym. Sci.*, 1983, **28**, 3849.
20. Hourston, D.J. and Zia, Y., *J. Appl. Polym. Sci.*, 1984, **29**, 629.
21. Yamanaka, K. and Inoue, T., *Polymer*, 1989, **30**, 662.
22. Kim, B.S., Chiba, T. and Inoue, T., *Polymer*, 1993, **34**, 2809.
23. Meijer, H.E.H., Venderbosch, R.W., Goossens, J.G.P. and Lemstra, P.J., *High Performance Polym.*, 1996, **8**, 1.
24. Borsig, E., Hrouz, J., Friedlerova, A. and Ilavsky, M., *J. Macromol. Sci. Chem. Edn.*, 1990, **A27**, 1613.
25. Borsig, E., Fiedlerova, A., Haüsler, K.G., Sambatra, R.M. and Michler, G.H., *Polymer*, 1993, **34**, 4787.
26. Borsig, E.B., Fiedlerova, A., Haüsler, K.G., Michler, G.H. and Greco, R., *Makromol. Chem. Makromol. Symp.*, 1994, **83**, 147.
27. EP Patent 0453999 A2.
28. Russell, T.P. and Koberstein, J.T., *J. Polym. Sci. Polym. Phys. Edn.*, 1983, **23**, 1109.
29. Koberstein, J.T. and Russell, T.P., *Macromolecules*, 1986, **19**, 714.
30. Galambos, A. F., Russell, T. P. and Koberstein, J. T., *Proceedings of the 18th NATAS Conference*. San Diego, CA, Sept. 24–27, 1989, Paper 39.
31. Ryan, A.J., Macosko, C.W. and Bras, W., *Macromolecules*, 1992, **25**, 6277.
32. Ryan, A.J., Stanford, J.L. and Tao, X.Q., *Polymer*, 1992, **34**, 4020.
33. Elwell, M.J., Mortimer, S. and Ryan, A.J., *Macromolecules*, 1994, **27**, 5428.
34. Bras, W., Derbyshire, G.E., Bogg, D., Cooke, J., Elwell, M.J., Komanschek, B.U., Naylor, S. and Ryan, A.J., *Science*, 1995, **267**, 996.
35. Kloosterboer, H., Serbutoviez, C., Boots, H. and Touwslager, F., *Polym. Mater. Sci. Eng.*, 1996, **74**, 190.
36. Bras, W., Derbyshire, G.E., Ryan, A.J., Mant, G.R., Felton, A., Lewis, R.A., Hall, C.J. and Greaves, G.N., *Nucl. Instrum. Methods Phys. Res. A*, 1993, **A326**, 587.
37. Barton, A. F. M., *CRC Handbook of Solubility Parameters and Other Cohesion Parameters*. CRC Press, Boca Raton, FL, 1991.
38. Quinn, F.A. and Mandelkern, L., *Macromolecules*, 1958, **80**, 3178.
39. Richards, R.B., *Trans. Faraday Soc.*, 1946, **42**, 10.
40. Roginova, L.Z. and Slonimskii, G.L., *Russian Chem. Rev.*, 1974, **43**, 1102.
41. Nakajima, A., Fujiwara, H. and Hamada, F., *J. Polym. Sci.: Part A2*, 1966, **4**, 507.
42. Goossens, J. G. P., Rastogi, S. and Meijer, H. E. H., *Proceedings of the 10th Annual Meeting Polymer Processing Society*. Akron, OH, USA, 5–8 April 1994.
43. Lipatov, Y.S., Grigor'yeva, O.P., Kovernick, G.P., Shilov, V. V and Sergryeva, L.M., *Makromol. Chem.*, 1985, **186**, 1401.
44. Cahn, J.W. and Hilliard, J.E., *J. Chem. Phys.*, 1958, **28**, 258.
45. van Krevelen, D. W., *Properties of Polymers: Correlations with Chemical Structure*, 3rd edn. Elsevier, Amsterdam, The Netherlands, 1991.
46. Ryan, A.J., Bras, W., Mant, G.R. and Derbyshire, G.E., *Polymer*, 1994, **35**, 4537.
47. Mitchell, G.R. and Windle, A.H., *Polymer*, 1984, **25**, 906.
48. Chu, B., Fytas, G. and Zalczer, G., *Macromolecules*, 1981, **14**, 395.
49. Chu, B. and Fytas, G., *Macromolecules*, 1982, **15**, 561.
50. Sears, W.M., Hunt, J.L. and Stevens, J.R., *J. Chem. Phys.*, 1981, **75**, 1599.
51. Gulari, E., McKeigue, K. and Ng, K.Y.S., *Macromolecules*, 1984, **17**, 1822.
52. Stokr, J. and Schneider, B., *J. Appl. Polym. Sci.*, 1979, **23**, 3553.
53. Strobl, G.R. and Hagedorn, W., *J. Polym. Sci.*, 1978, **16**, 1181.
54. Inaba, N., Sato, K., Suzuki, S. and Hashimoto, T., *Macromolecules*, 1986, **19**, 1690.
55. Inaba, N., Yamada, T., Suzuki, S. and Hashimoto, T., *Macromolecules*, 1988, **21**, 407.
56. Venderbosch, R. W., Ph.D. Thesis. Eindhoven University of Technology, The Netherlands, 1995.